https://doi.org/10.31436/iiumej.v25i1.3093

EXTENDABLE HIGH-GAIN DC-DC CONVERTER FOR STORAGE BATTERY AND PHOTOVOLTAIC CELL

S.M.A. MOTAKABBER, KHADIZA AKTER*, AHM ZAHIRUL ALAM AND SITI HAJAR YUSOFF

Department of Electrical and Computer Engineering, Kulliyyah of Engineering, International Islamic University Malaysia, Kuala Lumpur, Malaysia

**Corresponding author: khadiza@iubat.edu*

(Received: 12 October 2023; Accepted: 20 November 2023; Published on-line: 1 January 2024)

ABSTRACT: DC-DC converters with significant gain, ripple-free input current, and shared ground are required to elevate the output voltages of batteries, fuel cells, and Photovoltaic sources. The proposed topology utilizes a solitary switch to control the circuit and it has additional inculpation of a voltage doubler cell at the load side, a switch capacitor cell in the middle, and a quadratic cell at the output side. These cascaded configurations lead to significant voltage gains at moderate duty cycle rates. Additionally, the voltage stress over the power components is negligible, coming in under one-third of the resultant voltage. Moreover, the number of cells at the input and output side can be extended to obtain high voltage according to the requirements of the load. The gain in voltage, efficiency, and normalized voltage stress of the semiconductor elements in the circuit are examined concerning other solutions found in the literature. Eventually, photovoltaic and battery sources were included to analyze the proposed topology to confirm the circuit's multifaceted functionality. The circuit was developed for 270 W, 440 V output from 36 V input, and a 40 kHz switching pulse was used to drive the switch. The theoretical and simulation analysis states that incorporating photovoltaic and other sources did not deteriorate the transformation efficiency. Simulink and PSIM analysis found that the circuit successfully transferred 95% power from source to load.

ABSTRAK: Penukar DC-DC yang mempunyai gandaan ketara, input arus bebas riak dan pembumi berkongsi penting bagi meningkatkan voltan keluar bateri, sel bahan api dan sumber fotovolta. Topologi yang dicadangkan ini menggunakan suis tersendiri bagi mengawal litar dan ia mengandungi sel pendua voltan tambahan bagi menghentikan arus di bahagian beban, sel suis kapasitor di tengah dan sel kuadratik di bahagian voltan keluar. Konfigurasi berturutan ini membawa kepada gandaan voltan ketara pada kadar kitar tugas sederhana. Tambahan, tekanan voltan ke atas komponen kuasa boleh diabaikan, iaitu satu pertiga daripada voltan terhasil. Selain itu, bilangan sel di bahagian kemasukan dan keluaran arus boleh dilanjutkan bagi mendapatkan voltan tinggi mengikut keperluan beban. Gandaan voltan, kecekapan dan tekanan voltan ternormal pada bahan dalam litar semikonduktor diperiksa dengan menyamai penyelesaian lain yang ditemui dalam kajian terdahulu. Akhirnya, sumber fotovolta dan bateri dimasukkan bagi menganalisis topologi yang dicadangkan bagi mengesahkan fungsi pelbagai rupa litar. Litar yang dibangunkan ini digunakan pada kuasa 270 W, pada aras voltan 440 V dengan kemasukan voltan 36 V dan suis operasi berfrekuensi 40 kHz. Analisis teori dan simulasi menyatakan bahawa gabungan fotovolta dan sumber lain tidak mengurangkan kecekapan transformasi. Analisis Simulink dan PSIM mendapati litar ini berjaya memindahkan 95% kuasa dari sumber kepada beban.

KEYWORDS: *PV system; MPPT; DC-DC converter; voltage stress on semiconductor; CCM; DCM*

https://doi.org/10.31436/iiumej.v25i1.3093

1. INTRODUCTION

High voltage gain power electronic converters are crucial to the renewable energy system field because of their linking capability between RES and electrical power systems. They are widely used in electrical systems, including electric trains, satellites, electric vehicles, street lighting, battery charging, tracking a PV array's MPP, and high-voltage DC transmission [1]. The voltage output from a solar PV array or a fuel cell is rather low and contingent upon external conditions [2]. PV systems are designed in a series-parallel arrangement to obtain high output voltage. However, this configuration lowers efficiency and increases system size [3]. Hence, a high-boosting factor configured converter is used for these voltage-boosting applications because it can alter the converter's duty cycle to raise the voltage at the output to significantly higher levels relative to its input.

Figure 1 depicts the overall design of a DC grid-tied diagram using an HVG DC-DC step-up converter. As a result, various configurations of these kinds of topology have been put out in the literature to achieve the required voltage output [4].

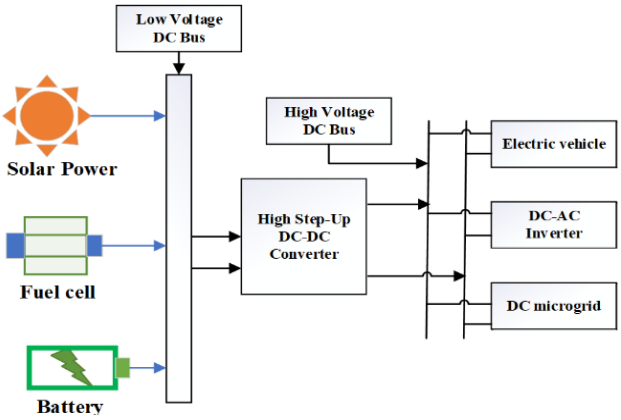

Fig. 1: Basic structure of the proposed converter applications.

These types of topologies can be classified as current-fed or voltage-fed, isolated or non-isolated, unidirectional or bidirectional, and soft-switched or hard-switched type. The transformer is used in an isolated converter topology to increase voltage at the input side by modifying its turn ratio [5]. On the other hand, these converters have a strong secondary side voltage overload and an excessive input current ripple content [6]. Furthermore, the two main disadvantages of isolated converters are leakage energy, heavy transformers, and multiple stages of the power conversion procedure [7]. As a result, non-isolated configurations such as Boost, Buck-Boost, CUK, and SEPIC converters are being utilized to adjust the system's performance [8,9]. They are commonly used because these converters are easy to use, affordable, effective, and have a wide variety of useful applications.

Many methods, such as the employment of a voltage multiplier, switched inductor, switched capacitor, etc., are employed to improve the functionality of high-gain converters. High-efficiency, step-up DC-DC converters have been presented in [10]. Active clamps have been used in these converters to recuperate leakage energy and lessen the problem with the diode's reverse recovery. The suggested converter in [11] obtained a considerable step-up voltage gain by combining a switching capacitor and two linked inductors. Furthermore, the reduced resistance had reduced conduction losses, thereby raising efficiency and lowering the diodes' reverse recovery.

https://doi.org/10.31436/iiumej.v25i1.3093

A highly effective method using dual-coupled inductors and an efficient step-up DC-DC converter for grid-tied solar systems has been demonstrated in [12]. Using a few extra auxiliary parts, a modified SEPIC circuit with a marginally greater gain than a boost converter has been described in [13]. Quadratic gain structures are introduced to boost the gain in [14] further, and when the duty ratio exceeds 70%, the quadratic converter produces higher gains. Consequently, inductor core saturation is a serious issue in these kinds of high-frequency operating converters. The voltage transformation can now be enhanced using quasi-z-source and z-source networks in conjunction with SC, SI, or other voltage-amplifying topologies. The converters described in [15] have higher element voltage stress and less gain in voltage. However, the converter's power density drops when more inductors are used. Additional boosting circuits and a dual switch-based flipping capacitor are employed to raise the gain. The topologies developed in [16] can attain high voltage gain (HVG) with higher efficiency. Nevertheless, the incorporation of a PV source deteriorates the input current smoothness and lessens the output voltage level. Moreover, most topologies are not compatible with tracking optimum power in the shortest time. Some topologies can track maximum power, but they offer high steady-state oscillation.

This brief proposes a single switched SC-employed non-isolated improved voltage gain DC-DC converter to address the shortcomings. Common ground, constant input current with little ripple content, HVG at varying duty ratios, and decreased voltage stress on components are all aspects of the suggested topology. With considerable efficiency, it can generate 440 V from 36 V of input even at a low-duty cycle. The steady-state investigation in DCM and CCM mode, the PV source implementation, MPP tracking analysis, performance comparison, and assessment are covered in the remaining sections of the study.

2. DESCRIPTION OF PROPOSED CIRCUIT

The suggested converter is being introduced to increase voltage gain using fewer components and reducing the stress caused by the voltage across the output semiconductor. The PV output is connected to the MOSFET switching circuit through an electric charge pump network. Finally, the output of the circuit uses a voltage doubler network and is connected to the load, as shown in Fig. 2. The circuit has two functioning modes since the MOSFET switch has two modes of operation: ON and OFF.

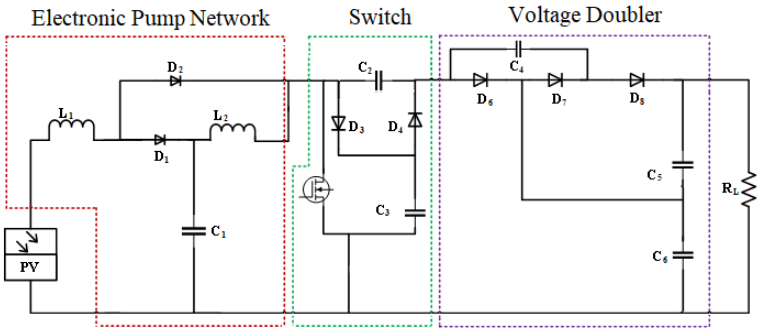

Fig. 2: Proposed design.

2.1 CCM Analysis of the Proposed Converter

When the converter operates in Continuous Conduction Mode (CCM), the current passing through the inductor never zeroes out throughout the switching cycle. It indicates that the inductor continuously receives current and is not completely discharged during the switching

https://doi.org/10.31436/iiumej.v25i1.3093

cycle's off-time. Designing DC-DC converters that are dependable and efficient requires the use of CCM analysis, particularly in situations where a steady and tightly monitored output voltage is required.

2.1.1 When Switch is ON ($0 \leq t \leq DT$)

When the MOSFET switch S is turned ON, the diodes D_2, D_4, D_6, and D_8 are forward-biased, and diodes D_1, D_3, and D_6 are reverse-biased, the flow direction in this situation is shown in Fig. 3. The PV energy is pumped to store in the L_1, simultaneously the storage energy of C_1 is pumped to store in the L_2. The output diode-capacitor doubler circuit is in action and increases the voltage across the load.

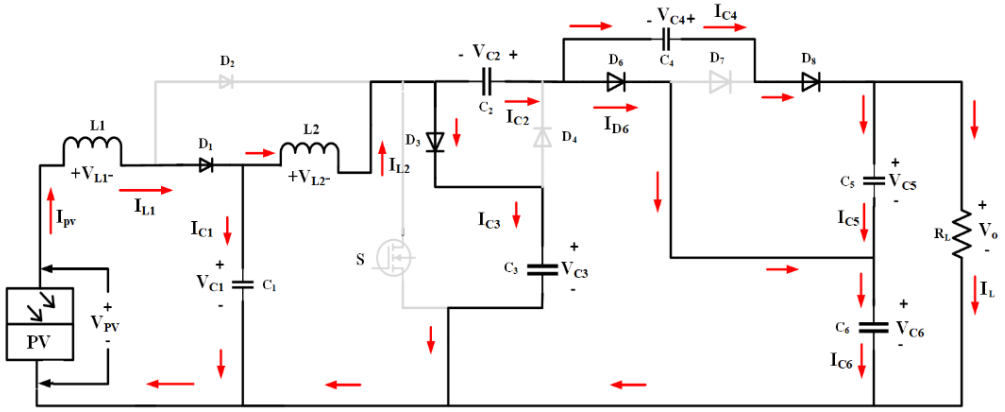

Fig. 3: Current flow direction when the MOSFET Switch is ON.

2.1.2 When Switch is OFF ($0 \leq t \leq DT$)

When the MOSFET switch is turned OFF, the diodes D_1, D_3, D_5, D_6 and D_7 are forward-biased, and the diodes D_2, D_4 and D_7 are reversed bias. Capacitors C_4 and C_5 are connected in parallel; thus, voltage drops across them are equal. Capacitor C_1 discharge through L_2 and stored the electrical energy for the next half cycle simultaneously. The capacitor C_4 discharge through the load, the current flow direction is shown in Fig. 4.

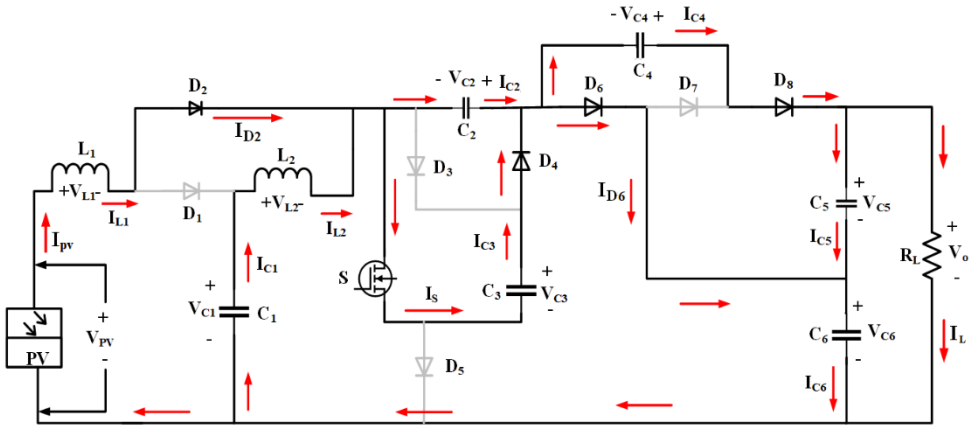

Fig. 4: Switch OFF operating principle.

2.1.3 Voltage Gain

The volt/sec change approach is implemented on the inductor to calculate the voltage gain.

https://doi.org/10.31436/iiumej.v25i1.3093

$$\int_0^{DT_S} V_{PV}\,dt + \int_{DT_S}^{T_S} (V_{PV} - V_{C1})\,dt = 0 \tag{1}$$

After solving the Eq. (1), the voltage across the capacitor C_1 can be calculated as,

$$V_{C1} = \frac{V_{PV}}{(1-D)} \tag{2}$$

Similarly, the voltage across the capacitor C_2 can be calculated as,

$$\int_0^{DT_S} V_{C1}\,dt + \int_{DT_S}^{T_S} (V_{C1} - V_{C2})\,dt = 0 \tag{3}$$

$$V_{C2} = \frac{V_{PV}}{(1-D)^2} \tag{4}$$

The output voltage across the load can be calculated as,

$$\therefore V_0 = \frac{3V_{in}}{(1-D)^2} \tag{5}$$

where D is the duty cycle of the switching frequency.

2.2 DCM Analysis of the Proposed Converter 0 ≤ t ≤ (1 − D − Dx)Ts

In discontinuous conduction mode (DCM), the current flowing through the inductor becomes zero. Hence, there will be no voltage drop across the inductor. As a result, no power is pulled from the source or the inductor. Both output capacitors C5 and C6 deliver current to the load. Figure 5 shows the operating diagram of DCM.

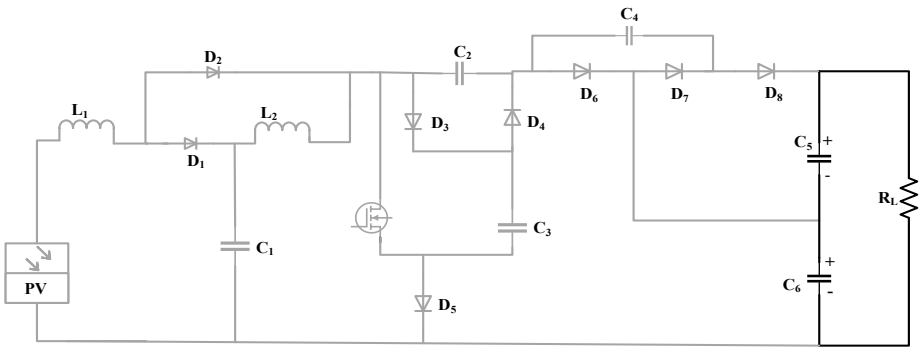

Fig. 5: DCM diagram of the circuit.

2.3 Ripple Current Computation

For a lossless circuit as an assumption, the equation of input and output power can be written as,

$$\begin{aligned} P_{PV} &= P_{out} \\ V_{PV} I_{PV} &= V_o I_o \end{aligned} \tag{6}$$

Considering the current through the L_1 inductor is equal to the input current Ipv

https://doi.org/10.31436/iiumej.v25i1.3093

$$\Delta I_L = \frac{DV_{PV}}{L(1-D)}(1-DT_S) \tag{7}$$

2.4 Assessment of Voltage Stresses on Semiconductor Device

The voltage stress across semiconductor devices appears during their reverse-biased state. For the first operating mode, the following voltage equation can be written as,

$$V_{D1} = V_{L2} \tag{8}$$

$$V_{L2} = V_{C1} \tag{9}$$

$$V_{C1} = \frac{V_{PV}}{(1-D)} \tag{10}$$

$$V_{D1} = \frac{V_{PV}}{(1-D)} \tag{11}$$

Similarly, the voltage stress across the other diodes is summarised in Table 1.

Table 1: Voltage stress across semiconductor components

Parameters	Voltage Stress	Parameters	Voltage Stress
V_{D1}	$\frac{V_{PV}}{(1-D)}$	V_{D5}	$\frac{V_o}{3}$
V_{D2}	$\frac{V_{PV}}{(1-D)}$	V_{D6}	$\frac{V_o}{3}$
V_{D3}	$\frac{V_{PV}}{(1-D)^2}$	V_{D7}	$\frac{V_o}{3}$
V_{D4}	$\frac{V_{PV}}{(1-D)^2}$	V_S	$\frac{V_{PV}}{(1-D)^2}$

3. PERFORMANCE OF THE CONVERTER WITH BATTERY SOURCE

MATLAB/Simulink and PSIM software simulated the recommended converters and validated the theoretical formulation. The parameters taken into account for the simulation are $V_{in} = 36$ V, $V_o = 440$ V, $D = 0.5$, $C_1 = 250$ µF, $C_2 = C_3 = 40$ µF, $C_4 = C_5 = C_6 = 100$ µF, $L_1 = L_2 = 2.5\ mH$ and $R_L = 750\ \Omega$. The switching frequency of the MOSFET switch is $40\ kHz$. Fig.7 displays the input-output voltage and current profile. The resultant $440V$ output voltage with 0.58 A current appeared across a $750\ \Omega$ load. The inductor current is $6.9A$, while the ripple current is 0.17 A, which is 2.4% of the average current. The average value of the voltage across C_1 is 72 V when the voltage over the rest of the capacitors is around 146V, the voltage between capacitors C_5 is increased to 150 V and becomes 292 V. Figure 6(a) and 6(b) show the proposed circuit's input voltage and current signal. Figure 6(c) and 6(d) demonstrate the output voltage and current.

The peak-to-peak output voltage difference is less than 0.25, which is a promising example of low fluctuation. The proposed topology has been incorporated with a 36 V battery source during simulation. The waveform characteristics of the proposed topology have been verified for voltage across each circuit element and semiconductor components. The simulation output of each component in terms of voltage and current flowing through them complies with the theoretically obtained output, as displayed in Fig. 6.

https://doi.org/10.31436/iiumej.v25i1.3093

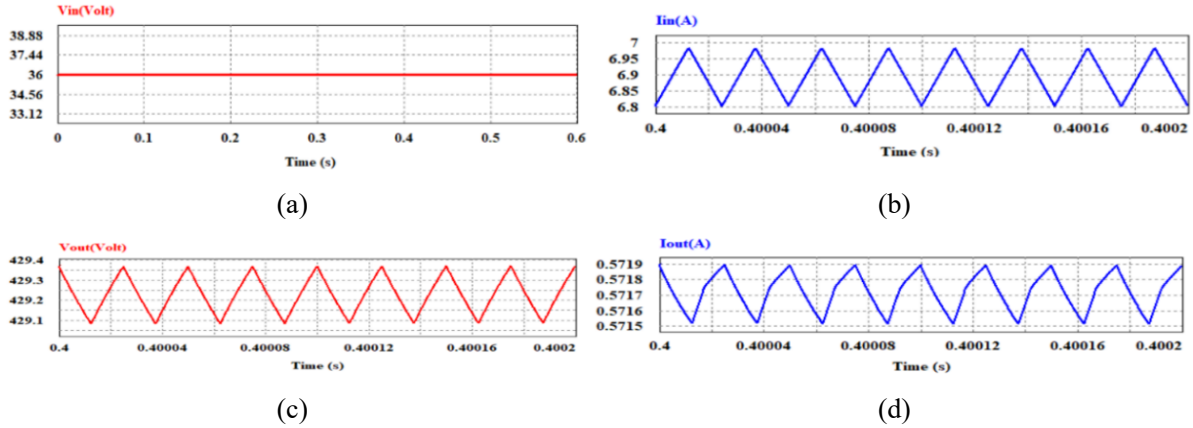

Fig. 6: Input voltage (a), Input current (b), output voltage (c) and output current waveform of proposed design.

4. PERFORMANCE OF THE CONVERTER WITH PV SOURCE

PV systems generally have intermittent characteristics, poor stability, and lower energy efficiency during conversion. The MPPT algorithm is required to guarantee that the solar energy system can produce the most electricity possible. The proposed design has been incorporated with the PV source to ensure the optimum power obtained from the PV source. Two parallel strings are used for simulation, each containing three modules. The maximum power of the PV panel is 1050.55 watts, shown in the PV curve of Fig. 7. The Perturb and Observe (P&O) algorithm has been utilized to ensure the tracking of optimum power [17].

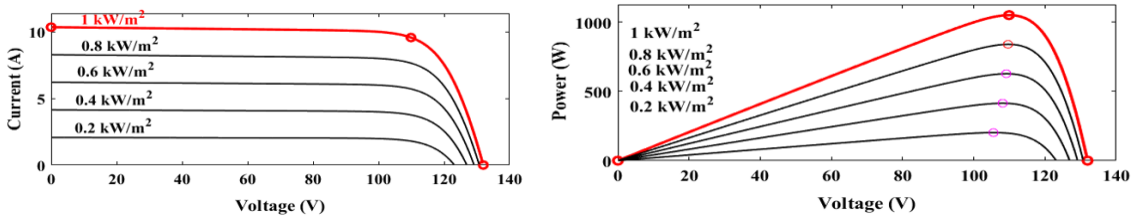

Fig. 7: Characteristics of the implemented solar module (a) I-V and (b) P-V.

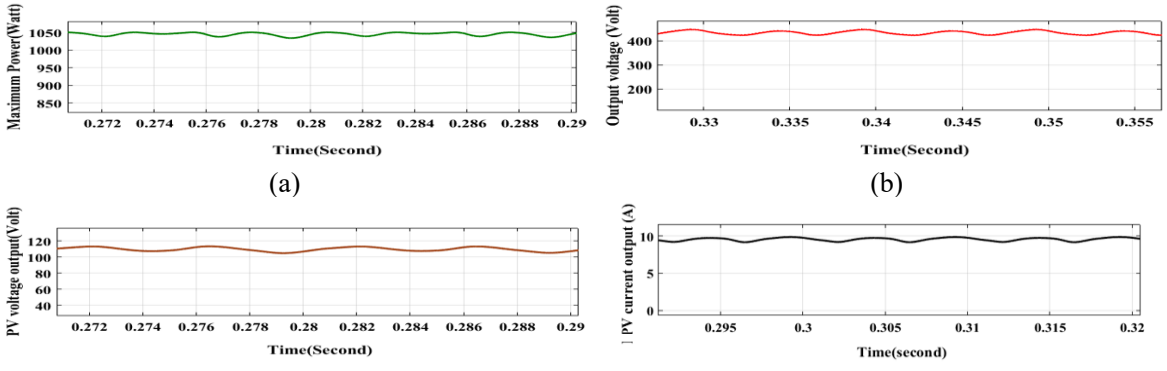

Fig. 8: Graphical representation of the proposed system (a) MPP module, (b) converter output voltage, (c) PV output voltage and (d) PV output current.

https://doi.org/10.31436/iiumej.v25i1.3093

Figure 8(a) shows the proposed converter tracking efficiency capability with less tracking time and less steady-state oscillation. Incorporating the MPPT controller did not affect the boosting factor of the circuit. Figure 8(b) shows the converter output voltage, which complies with the battery output voltage. The PV current and voltage waveform are demonstrated in Fig. 8(c) and (d), which show the resemblance of the I-V curve in Fig. 7(a).

5. COMPARATIVE ANALYSIS

The suggested converter was contrasted with its more recent counterpart to verify the viability of the recommended converters successfully. Eight recently developed step-up converter circuits were compared. A detailed comparison is made between the various features of these converters concerning voltage across semiconductors, efficiency, and boost factor. Figures 9, 10, 11 graphically represent the performance of different circuit topologies, including the proposed design. In the figure, the x-axis number within the square bracket represents the reference number of the article to home compared to the proposed design.

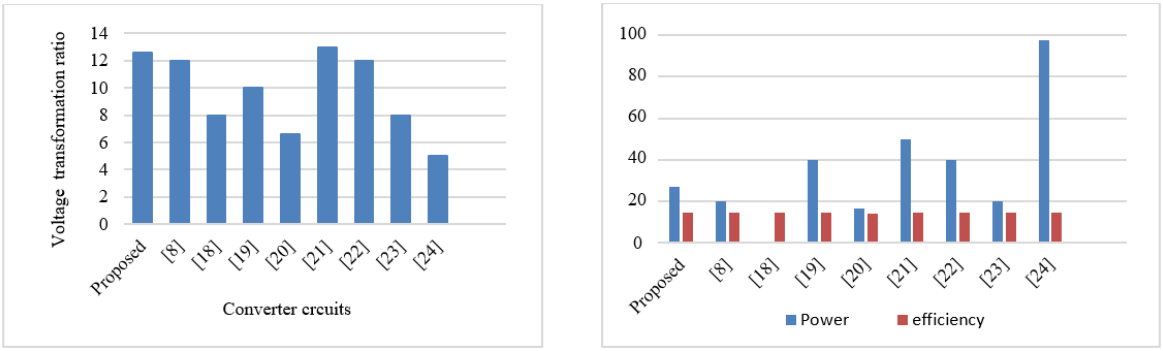

(a) (b)

Fig. 9: Performance of various topologies (a) voltage boosting and (b) efficiency concerning power comparison.

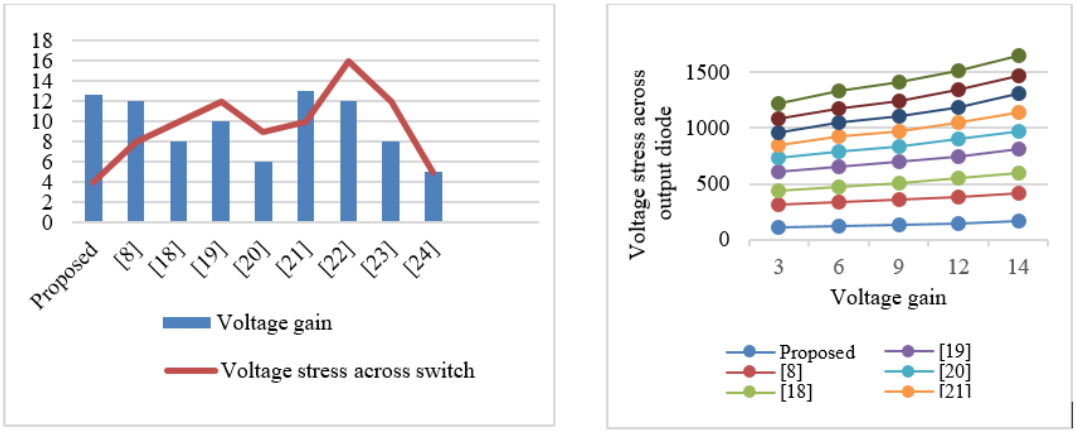

(a) (b)

Fig. 10: Represents (a) voltage gain concerning voltage stress and (b) voltage stress comparison of various topologies.

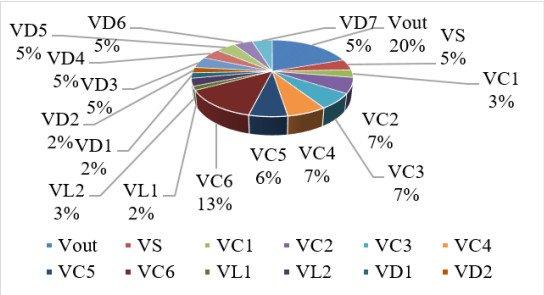

Fig. 11: Percentage voltage drops across each element of the proposed topology.

6. CONCLUSION

This paper proposes a unique design of non-isolated boost topology with a large conversion efficiency. A thorough discussion of the theoretical analysis and operating principles is provided in detail here. With neither an excessive duty cycle nor a high turns ratio, the suggested converter has been effectively built to obtain an extremely high step-up voltage gain. The suggested converter's construction might be expanded by increasing the QC and VDC cell to attain a greater step-up voltage boosting range. A significant reduction in the voltage stress on semiconductors was observed concerning gain. The primary side's quadratic structure contributed to a notable reduction in the input current fluctuation. Having low distortion in input current the proposed topology could efficiently track the optimum power of the PV panel without deteriorating circuit transformation efficiency. The circuit transformation efficiency was found to be 95%, whereas 98% transformation efficiency was observed for MPPT. A comparison between the suggested converter and other recently developed topologies is provided for better justification. The result analysis section complies with the similarity between analytical and simulation output. Considering all these merits, the suggested converter is ideally suited for integrating RES and battery sources, which requires high effectiveness and voltage enhancement.

ACKNOWLEDGEMENT

This research has been supported by the Engineering Merit Scholarship Scheme 2021 and Research Management Centre, International Islamic University Malaysia.

REFERENCES

[1] Forouzesh M, Siwakoti YP, Gorji SA, Blaabjerg F, Lehman B. (2017) Step-Up DC-DC converters: A comprehensive review of voltage-boosting techniques, topologies, and applications. IEEE Trans. Power Electron., 32(12): 9143-9178. doi: 10.1109/TPEL.2017.2652318

[2] Kolli A, Gaillard A, De Bernardinis A, Bethoux O, Hissel D, Khatir Z. (2015) A review on DC/DC converter architectures for power fuel cell applications. Energy Convers. Manag., 105: 716-730. doi: 10.1016/j.enconman.2015.07.060.

[3] Esram T, Chapman PL. (2007) Comparison of photovoltaic array maximum power point tracking techniques. IEEE Trans. Energy Convers., 22(2): 439-449. doi: 10.1109/TEC.2006.874230

[4] Gopinathan S, Rao VS, Sundaramoorthy K. (2022) Family of nonisolated quadratic high gain DC-DC converters based on extended capacitor-diode network for renewable energy source integration. IEEE J. Emerg. Sel. Top. Power Electron., 10(5): 6218-6230. doi: 10.1109/JESTPE.2022.3167283

[5] Kasper M, Ritz M, Bortis D, Kolar JW. (2013) PV panel-integrated high step-up high efficiency isolated GaN DC-DC boost converter. INTELEC, Int. Telecommun. Energy Conf., pp. 602-608.
[6] Hasanpour S, Forouzesh M, Siwakoti Y, Blaabjerg F. (2021) A new high-gain, high-efficiency SEPIC-based energy applications. IEEE Journal of Emerging and Selected Topics in Industrial Electronics, 2(4): 567-578. doi: 10.1109/JESTIE.2021.3074864
[7] Nguyen MK, Duong TD, Lim YC. (2018) Switched-capacitor-based dual-switch high-boost DC-DC converter," IEEE Trans. Power Electron., 33(5): 4181-4189. doi: 10.1109/TPEL.2017.2719040.
[8] Hasanpour S, Nouri T, Blaabjerg F, Siwakoti YP. (2023) High step-up SEPIC-based trans-inverse DC-DC converter with quasi-resonance operation for renewable energy applications. IEEE Trans. Ind. Electron., 70(1): 485-497. doi: 10.1109/TIE.2022.3150103.
[9] Sarikhani A, Allahverdinejad B, Hamzeh M. (2021) A nonisolated buck-boost DC-DC converter with continuous input current for photovoltaic applications. IEEE J. Emerg. Sel. Top. Power Electron., 9(1): 804-811. doi: 10.1109/JESTPE.2020.2985844
[10] Rajabi A, Rajaei A, Tehrani VM, Dehghanian P, Guerrero JM, Khan B. (2022) A nonisolated high step-up DC-DC converter using voltage lift technique: Analysis, design, and implementation. IEEE Access, 10: 6338-6347. doi: 10.1109/ACCESS.2022.3141088
[11] Alghaythi ML, O'Connell RM, Islam NE, Khan MMS, Guerrero JM. (2020) A high step-up interleaved DC-DC converter with voltage multiplier and coupled inductors for renewable energy systems. IEEE Access, 8: 123165-123174. doi: 10.1109/ACCESS.2020.3007137
[11] Forouzesh M, Shen Y, Yari K, Siwakoti YP, Blaabjerg F. (2017) High-efficiency high step-up DC-DC converter with dual coupled inductors for grid-connected photovoltaic systems. IEEE Trans. Power Electron., 33(7): 5967-5982. doi: 10.1109/TPEL.2017.2746750
[12] Ansari SA, Moghani JS. (2019) A novel high voltage gain noncoupled inductor SEPIC converter. IEEE Trans. Ind. Electron., 66(9): 7099-7108. doi: 10.1109/TIE.2018.2878127
[13] Jalilzadeh T, Rostami N, Babaei E, Maalandish M. (2023) Nonisolated topology for high step-up DC-DC converters. IEEE J. Emerg. Sel. Top. Power Electron., 11(1): 1154-1168. doi: 10.1109/JESTPE.2018.2849096
[14] Haji-Esmaeili MM, Babaei E, Sabahi M. (2018) High step-up quasi-Z source DC-DC converter. IEEE Trans. Power Electron., 33(12): 10563-10571. doi: 10.1109/TPEL.2018.2810884
[15] Jiya IN, Van Khang H, Kishor N, Ciric RM. (2022) Novel family of high-gain nonisolated multiport converters with bipolar symmetric outputs for DC microgrids. IEEE Trans. Power Electron., 37(10): 12151-12166. doi: 10.1109/TPEL.2022.3176688
[16] Gopinathan S, Rao VS, Kumaravel S. (2023) Enhanced voltage gain boost DC-DC converter with reduced voltage stress and core saturation. IEEE Trans. Circuits Syst. II Express Briefs, 70(8): 3019-3023. doi: 10.1109/TCSII.2023.3252721
[17] Verma D, Nema S, Agrawal R, Sawle Y, Kumar A. (2022) A different approach for maximum power point tracking (MPPT) using impedance matching through nonisolated DC-DC converters in solar photovoltaic systems. Electron., 11(7): 1053. doi: 10.3390/electronics11071053.
[18] Shahrukh K, Mohammad Z, Arshad M, Abbas S. N, Javed A, Mamdouh L. A, Basem A, Mohd T, Adil S and Chang-Hua L. (2021) A new transformerless ultra high gain DC-DC converter for DC microgrid application. IEEE Access, 9: 124560-124582. doi: 10.1109/ACCESS.2021.3110668.
[19] Gopinathan S, Rao VS, KS. (2023) Enhanced voltage gain boost DC-DC converter with reduced voltage stress and core saturation. IEEE Trans. Circuits Syst. II Express Briefs, 70(8), 3019-3023, doi: 10.1109/TCSII.2023.3252721.
[20] Subhani N, May Z, Alam MK, Khan I, Hossain MA, Mamun S. (2023) An improved nonisolated quadratic DC-DC boost converter with ultra high gain ability. IEEE Access, 11: 11350-11363. doi: 10.1109/ACCESS.2023.3241863

[21] Li H, Du H, Zeng Y, Qiu Z, Jiang X, Chen Z. (2022) A modified interleaved capacitor clamped DC-DC converter with non-resonant soft switching. IEEE Trans. Power Electron., 37(10): 12221-12236. doi: 10.1109/TPEL.2022.3163010.

[22] Sadaf S, Al-Emadi N, Maroti PK, Iqbal A. (2021) A new high gain active switched network-based boost converter for DC microgrid application. IEEE Access, 9: 68253-68265. doi: 10.1109/ACCESS.2021.3077055

[23] Nouri T, Hosseini SH, Babaei E. (2014) Analysis of voltage and current stresses of a generalized step-up DC-DC converter. IET Power Electron., 7(6): 1347-1361. doi: 10.1049/iet-pel.2013.0496

[24] Bao D, Kumar A, Pan X, Xiong X, Beig AR, Singh SK. (2021) Switched inductor double switch high gain DC-DC converter for renewable applications. IEEE Access, 9: 14259-14270. doi: 10.1109/ACCESS.2021.3051472.